The Galactic Center: Feeding and Feedback in a Normal Galactic Nucleus
Proceedings IAU Symposium No. 303, 2013
L. O. Sjouwerman, C. C. Lang & J. Ott

doi:10.1017/S174392131400012X

Formation of nuclear rings of barred galaxies and star formation therein

Woong-Tae Kim, Woo-Young Seo and Yonghwi Kim

Center for the Exploration of the Origin of the Universe (CEOU), Astronomy Program, Department of Physics & Astronomy, Seoul National University, 1 Gwanak-Ro, Gwanak-Gu, Seoul 151-742, Republic of Korea
email: wkim@astro.snu.ac.kr, seowy@astro.snu.ac.kr, kimyh@astro.snu.ac.kr

Abstract. Barred galaxies contain substructures such as a pair of dust lanes and nuclear rings, with the latter being sites of intense star formation. We study the substructure formation as well as star formation in nuclear rings using numerical simulations. We find that nuclear rings form not by the Lindblad resonances, as previously thought, but by the centrifugal barrier that inflowing gas along dust lanes cannot overcome. This predicts a smaller ring in a more strongly barred galaxy, consistent with observations. Star formation rate (SFR) in a nuclear ring is determined primarily by the mass inflow rate to the ring. In our models, the SFR typically shows a short strong burst associated with the rapid gas infall and stays very small for the rest of the evolution. When the SFR is low, ages of young star clusters exhibit an azimuthal gradient along the ring since star formation takes place mostly near the contact points between the dust lanes and the nuclear ring. When the SFR is large, on the other hand, star formation is widely distributed throughout the whole length of the ring, with no apparent age gradient of star clusters. Since observed ring star formation appears long-lived with episodic bursts, our results suggest that the bar region should be replenished continually with fresh gas from outside.

Keywords. galaxies: ISM — galaxies: kinematics and dynamics — galaxies: nuclei — galaxies: spiral — ISM: general — shock waves — stars: formation

1. Introduction

Barred galaxies are common in the universe. Observations indicate that about 30% of luminous disk galaxies in the local universe (with the redshift z up to ~ 0.2) have relatively strong bars in the central regions (e.g., Sheth *et al.* 2008; Masters *et al.* 2011; Lee *et al.* 2012). The bar fraction increases to 65% if weakly barred galaxies are included, and decreases with increasing z (e.g., Sheth *et al.* 2008). Our own Milky Way also possesses a relatively short and weak bar.

A stellar bar has a dramatic influence on gas evolution in disk galaxies by providing non-axisymmetric torque, leading to the formation of bar substructures such as a pair of dust lanes at the leading sides of the bar, a nuclear ring near the galaxy center, and nuclear spirals inside the ring (e.g., Sanders & Huntley 1976; Athanassoula 1992; Buta & Combes 1996; Martini *et al.* 2003; Prieto *et al.* 2005; Comerón *et al.* 2009; Hsieh *et al.* 2011). Dust lanes are regions of compressed gas in shocks produced by the bar potential, through which the gas in the bar regions infalls to the central part (Athanassoula 1992; Kim *et al.* 2013b). Nuclear rings are sites of intense star formation (e.g., Buta & Combes 1996; Knapen *et al.* 2006; Mazzuca *et al.* 2008; Comerón *et al.* 2010; Sandstrom *et al.* 2010; Mazzuca *et al.* 2011). Nuclear spirals are thought to be a channel for gas accretion to the galaxy center to fuel a central black hole (e.g., Shlosman *et al.* 1990; van de Ven & Fathi 2010).

Physical properties of bar substructures differ considerably from galaxy to galaxy. Some galaxies have relatively straight dust lanes, while others have more curved ones (e.g., Athanassoula 1992). For example, the dust lanes in NGC 6951 have a curvature angle of $\Delta\alpha = 9°$, while $\Delta\alpha = 73°$ in NGC 4321 (e.g., Comerón *et al.* 2009). Nuclear rings in some galaxies are small in radius ($R_{\rm ring} \sim 0.2$kpc in NGC 1300), while others such as NGC 1343 have $R_{\rm ring} \sim 1$kpc (e.g., Comerón *et al.* 2010). Some galaxies such as NGC 2997 have tightly wound nuclear spirals, while others such as NGC 1097 have relatively loosely wound ones (e.g., Peeples & Martini 2006).

What determines these properties of bar substructures? Regarding nuclear rings, in particular, it has been commonly accepted that they form by the resonant interactions of the gas with the underlying bar potential (e.g., Combes & Gerin 1985; Knapen *et al.* 1995; Buta & Combes 1996; Comerón *et al.* 2010). This idea was presumably motivated by the observational result that most nuclear rings are found close to the inner Lindblad resonance (ILR) radius. However, there are several physical arguments against the ring formation by the resonance. First, the bar torque near the galaxy center is very weak compared to other forces such as centrifugal forces and ram pressure forces of the inflowing gas, so that the bar potential itself is unlikely to be important for the ring formation. Second, resonance is a secular process occurring very slowly, while the time scale of the ring formation in numerical modeling is only of order of ~ 0.1 Gyr. Third, material receiving periodic kicks is expelled from the resonance locations, as gaps in planetary rings and the asteroid belt in the solar system illustrate. All of these suggest that the ring formation is not governed by the resonance.

To understand the formation of bar substructures and star formation occurring in nuclear rings, we have been investigating gas dynamical evolution of barred galaxies using high-resolution numerical simulations. Our numerical studies extend the pioneering work of Athanassoula (1992) by exploring the effects of the gas sound speed and the presence of a central supermassive black hole (Kim *et al.* 2012b), magnetic fields (Kim & Stone 2012), and varying bar strength (Kim *et al.* 2012a). We have also been studying star formation in nuclear rings by utilizing a prescription for star formation and associated feedback effects (Seo & Kim 2013). In this article, we summarize the highlights of these works, focusing on the formation of nuclear rings and star formation therein. The reader is referred to the papers mentioned above for technical details as well as more quantitative results.

2. Model and method

Following Athanassoula (1992), we consider a very simple galaxy model in which the external gravitational potential responsible for disk rotation consists of a stellar disk, a bulge/halo with mass $M_{\rm bul}$, a stellar bar with mass $M_{\rm bar}$, and a central black hole with mass $\mathrm{M}_\bullet = 4\times10^7\ \mathrm{M}_\odot$. We fix the total mass of the spheroidal component (bar plus bulge/halo) to $M_{\rm bar} + M_{\rm bul} = 5 \times 10^{10}\ \mathrm{M}_\odot$ inside $R = 10$ kpc, which gives rise to an almost-flat rotation curve with the rotational velocity $v_c = 200\ \mathrm{km\,s^{-1}}$ at outer parts. The bar potential is modeled by a Ferrers prolate spheroid characterized by its mass, the index n representing central density concentration, the semi-major and minor axes a and b, and its pattern speed Ω_b. We consider an infinitesimally-thin, unmagnetized, self-gravitating gaseous disk with initially-uniform surface density Σ_0, and place it under the external potential to study its dynamical responses to the bar potential. For simplicity, we take an isothermal equation of state with the sound speed of $c_s = 10\ \mathrm{km\,s^{-1}}$.

For the bar potential, we fix $n = 1$ and $a = 5$ kpc, and vary $M_{\rm bar}$ and b using two dimensionless parameters: the bar mass fraction $f_{\rm bar} = M_{\rm bar}/(M_{\rm bar} + M_{\rm bul})$ within

https://doi.org/10.1017/S174392131400012X Published online by Cambridge University Press

$R = 10$ kpc and the aspect ratio $\mathcal{R} = a/b$. To explore diverse galactic conditions with varying bar strength, we consider models with differing $f_{\rm bar}$ between 0.08 and 0.6 and $\mathcal{R}$ between 1.5 and 3.5. We take $\Omega_b = 33\ {\rm km\,s^{-1}\,kpc^{-1}}$. The corresponding corotation resonance radius is 6 kpc. The presence of the black hole at the galaxy center allows only one ILR at $R_{\rm ILR} \sim 1.3 - 2.2$ kpc depending on $f_{\rm bar}$ and $\mathcal{R}$ (Kim *et al.* 2012a).

We solve the equations of ideal hydrodynamics using the grid-based CMHOG code in cylindrical geometry in a frame corotating with the bar. The code is third-order accurate in space and has very little numerical diffusion (Piner *et al.* 1995). To resolve the central regions with high accuracy, we set up a logarithmically-spaced grid that extends from $R = 0.04$ kpc to 16 kpc. The number of zones in our models is 1024 in the radial direction and 535 in the azimuthal direction covering the half-plane. The corresponding spatial resolution is 0.2 pc at the inner boundary, 6 pc at $R = 1$ kpc where a nuclear ring typically forms, and 94 pc at the outer radial boundary. We adopt outflow and continuous boundary conditions at the inner and outer radial boundaries, respectively, and the periodic conditions at the azimuthal boundaries.

For models with star formation and feedback included, we incorporate a prescription that includes the critical density corresponding to the Jeans condition, a star formation efficiency of $\epsilon = 1\%$ (Krumholz & Tan 2007), 90% conversion of the gas mass to newly-formed stellar particles representing star clusters, and delayed feedback via supernova explosions in the form of momentum injection, with the delay time of 10 Myr. The amount of momentum that goes into the in-plane direction by $\mathcal{N}$ simultaneous supernova events from a single cluster is taken to be $\sim 2.25 \times 10^5 \mathcal{N}^{7/8} (\Sigma/1\ {\rm M_\odot\ pc^{-2}})^{-1/4}\ {\rm M_\odot\ km\,s^{-1}}$ (Kim *et al.* 2012a; see also Shull 1980; Kim *et al.* 2011).

3. Bar strength

As we will show in the next section, it is the bar strength that controls the physical properties of bar substructures. It has been customary to define the bar strength as

$$Q_b \equiv \left. \frac{F_T}{F_R} \right|_{\rm max}, \tag{3.1}$$

where F_T is the tangential force due to the bar and F_R is the centrifugal force of the galaxy rotation (e.g., Combes & Sanders 1981; Laurikainen & Salo). Assuming that the galaxy has a flat rotation curve and is dominated by the spheroidal component, one can show for $n = 1$ Ferrers prolate bars that

$$Q_b = \frac{15}{32} \frac{a C_0^2}{\sqrt{C_x C_y}} f_{\rm bar}, \tag{3.2}$$

which occurs at the galactocentric radius

$$R_{\rm max} = \frac{(-C_0)^{1/2}}{2} \left(\frac{1}{C_x} + \frac{1}{C_y} \right)^{1/2}, \tag{3.3}$$

(Kim *et al.* 2012). Here, $C_0 = W_{10} - W_{01} \leqslant 0$, $C_x = W_{02} - W_{11} \geqslant 0$, and $C_y = W_{11} - W_{20} \geqslant 0$, with W_{ij}'s being the coefficients of the $x^{2j} y^{2i}$ terms in the expansion of the bar potential (Pfenniger 1984). No analytic expression is available when $n \neq 1$.

Since real bars may have the concentration index n different from unity and galaxy rotation curves are not exactly flat, we use our galaxy models to calculate Q_b and $R_{\rm max}$ by varying $f_{\rm bar}$, $\mathcal{R}$, and n. Figure 1 plots the results with $f_{\rm bar} = 0.3$ as various lines. The analytic results (equations [3.2] and [3.3]) for $n = 1$ and $f_{\rm bar} = 0.3$ are in good agreement

https://doi.org/10.1017/S174392131400012X Published online by Cambridge University Press

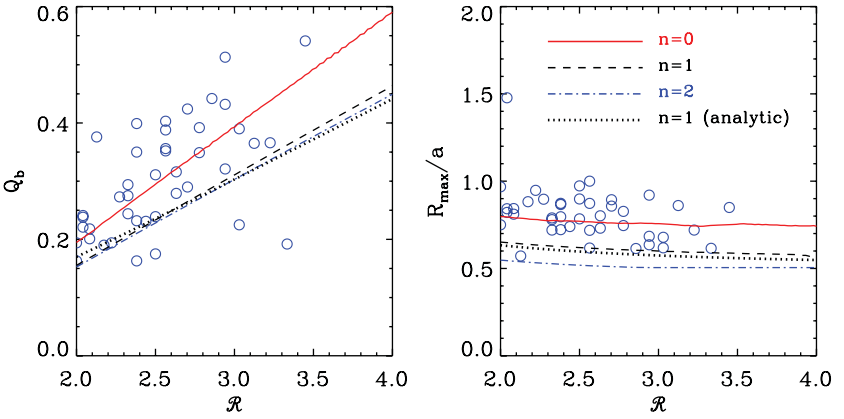

Figure 1. Dependence of (**left**) the bar strength Q_b and (**right**) the radius $R_{\rm max}$ of the maximum bar torque upon the bar aspect ratio $\mathcal{R}$. The results with $f_{\rm bar} = 0.3$ for our galaxy models are shown as various lines. Open circles plot the observational results taken from Comerón *et al.* (2010). Adopted from Kim *et al.* (2012a). [A color version is available online.]

with the numerical results. Plotted as open circles are the observational results adopted from Comerón *et al.* (2010) for nearly barred galaxies. Note that there are few galaxies with $\mathcal{R} > 3.5$. Note also that Q_b increases with $\mathcal{R}$, while $R_{\rm max}$ is relatively insensitive to $\mathcal{R}$. For observed galaxies with $R_{\rm max}/a > 1$, the Q_b parameter is governed by spiral arms rather than the bar. It is apparent from Figure 1 that if the observed bars are approximated by Ferrers prolate spheroids, they are less concentrated toward the center than $n = 1$ and most likely have the mass fraction of $f_{\rm bar} \simeq 0.3$.

4. Formation of nuclear rings

Since gas in galaxies is very responsive, the imposed bar potential can make its orbits easily deviate from circular motions, eventually forming dust-lane shocks at the leading side of the bar major axis. The gas passing through the shocks loses angular momentum and thereby moves toward the central region. The infalling gas starts to rotate faster gradually as it follows perturbed epicycle orbits, and forms a nuclear ring at the location where centrifugal force balances the gravity (Kim *et al.* 2012a). At the same time, the gas near the center (inside the ring) is perturbed weakly by the bar potential that is nearly axisymmetric, developing nuclear spirals that grow stronger with time.

Figure 2 plots density distributions at $t = 0.3$ Gyr in models with (left) $f_{\rm bar} = 0.08$, (middle) 0.15, and (right) 0.3 in the central (top) 5 kpc and (bottom) 2 kpc regions, respectively. All the models have $\mathcal{R} = 2.0$ and $\Sigma_0 = 10$ $\mathrm{M}_\odot$ pc^{-2}. Note that dust lanes follow some x_1 orbits, shown as solid ovals in the upper panels, and tend to be more straight in models with a stronger bar, although they are quite weak at this time. This is consistent with the previous theoretical results of Athanassoula (1992) and the observational results of Knapen *et al.* (2002) and Comerón *et al.* (2009). Notice that only the gas inside the outermost x_1 orbit that cuts the x- and y-axes at $x_c = 3.6$ kpc and $y_c = 4.7$ kpc responds to the bar potential dramatically, resulting in radial gas inflows. Outside the outermost x_1 orbit, on the other hand, the bar potential is not strong and the gas simply moves on slightly perturbed, near circular orbits, without inducing shocks.

https://doi.org/10.1017/S174392131400012X Published online by Cambridge University Press

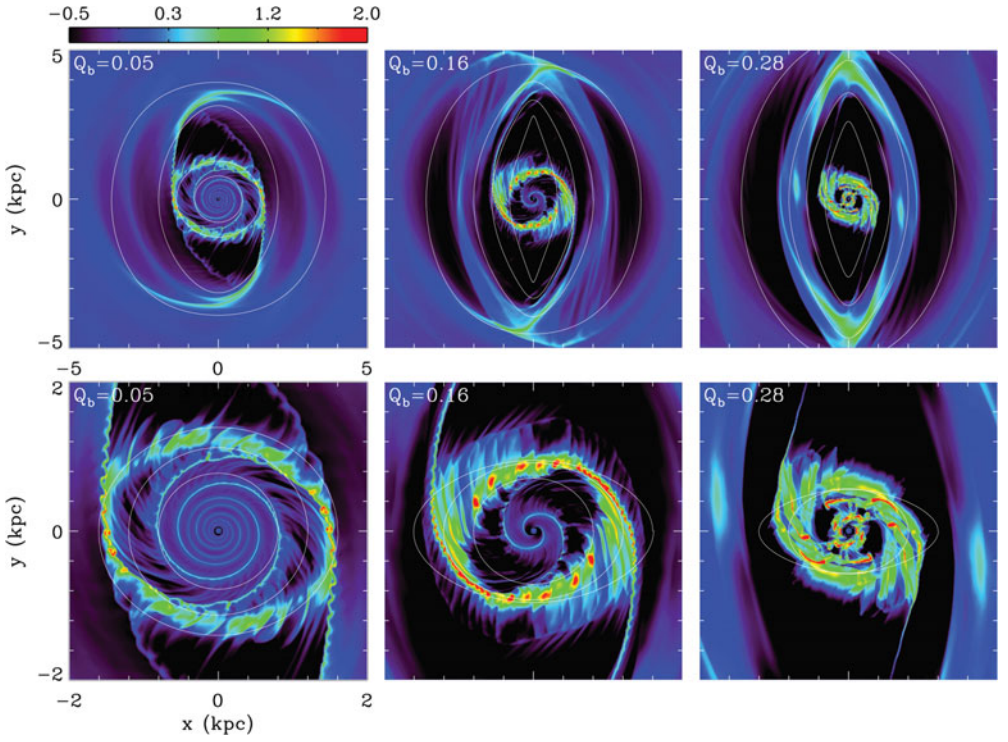

Figure 2. Snapshots of gas surface density in logarithmic scale for models with $Q_b = 0.05$ ($f_{\rm bar} = 0.08$ and $\mathcal{R} = 2.0$), $Q_b = 0.16$ ($f_{\rm bar} = 0.15$ and $\mathcal{R} = 2.0$), and $Q_b = 0.28$ ($f_{\rm bar} = 0.30$ and $\mathcal{R} = 2.0$) from left to right, respectively, at $t = 0.3$ Gyr in the central (**top**) $R = 5$ kpc and (**bottom**) 2 kpc regions. The solid ovals draw the x_1 orbits that cut the x-axis at $x_c = 0.8$, 1.4, 2.0, and 3.6 kpc in the upper panels and the x_2 orbits with $x_c = 0.8$, 1.2, 1.6 kpc in the lower panels except for the $Q_b = 0.28$ model where two x_2 orbits with $x_c = 0.8$ and 1.2 kpc are shown. Colorbar labels $\log(\Sigma/\Sigma_0)$. Adopted from Kim *et al.* (2012a). [A color version is available online.]

Other than weak trailing spirals that emerge from the bar ends, the outer regions are almost featureless.

From Figure 2, it is clear that more strongly barred galaxies have a smaller nuclear ring that closely follows some x_2 orbits, shown as solid ovals in the lower panels. We directly measure the radius, $R_{\rm ring}$, of the ring in each model and take its time average. Figure 3 plots the mean values (squares) and standard deviations (errorbars) of the ring radius as a function of Q_b, relative to the ILR radius $R_{\rm ILR}$ in the left panel and to the bar semi-major axis in the right panel. Note that $R_{\rm ring}/R_{\rm ILR}$ is well less than unity and becomes smaller with increasing Q_b, evidencing that the ring formation is not due to the ILR. Our best fits are $R_{\rm ring}/R_{\rm ILR} = 0.2Q_b^{-0.40}$ and $R_{\rm ring}/a = 0.06Q_b^{-0.51}$, plotted as solid lines. In Figure 3(b), the observational ring sizes (open circles) adopted from Comerón *et al.* (2010) are compared to our numerical results. For $Q_b < 0.15$, the agreement between the observational and numerical results is excellent. For $Q_b > 0.15$, the ring size in our models corresponds roughly to the upper envelope of the observational results. Overall, the tendency of having a smaller nuclear ring in a more strongly barred galaxy is the same in both observational and numerical results. Physically, this is because a stronger bar induces stronger dust-lane shocks, hence capable of removing larger amount of angular

https://doi.org/10.1017/S174392131400012X Published online by Cambridge University Press

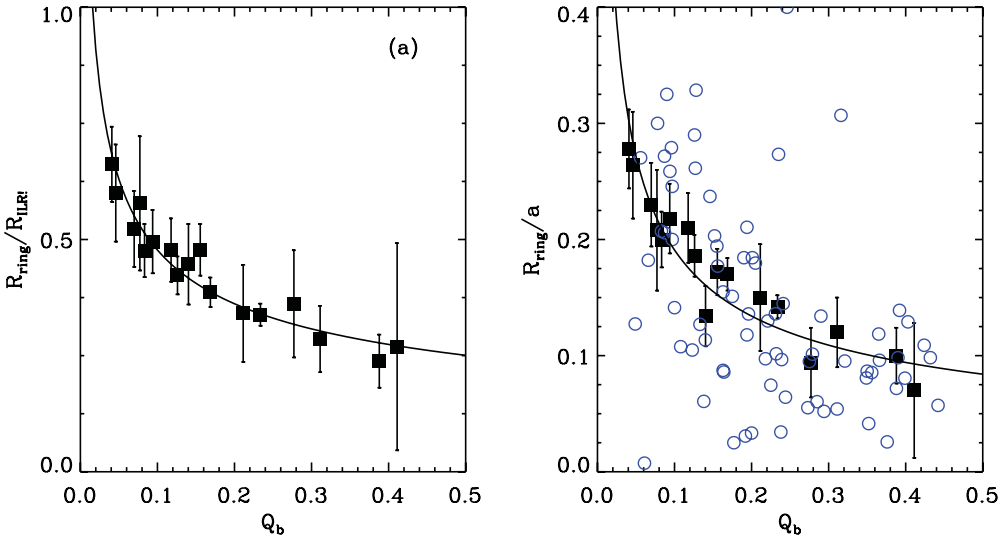

Figure 3. Mean values (squares) and standard deviations (errorbars) of the ring radius $R_{\rm ring}$ averaged over $t = 0.3 - 1.0$ Gyr in our numerical models, relative to **(a)** the ILR radius and **(b)** the bar semi-major axis, as functions of the bar strength. In **(b)**, open circles represent the observed ring sizes taken from Comerón *et al.* (2010). The solid lines are the best fits, given in the text. See Kim *et al.* (2012a). [A color version is available online.]

momentum from the gas. Consequently, the postshock gas can move closer to the galaxy center before encountering the centrifugal barrier, resulting in a smaller ring.

The bottom panels in Figure 2 also show that nuclear spirals are all trailing in shape, and are more loosely wound in more strongly-barred galaxies. Buta & Combes (1996) found that the shape of nuclear spirals is determined by the rotation curve, such that they are leading (trailing) in the region where $d(\Omega-\kappa/2)/dR$ is positive (negative). Here, Ω and κ refer to the angular and the epicycle frequencies of galaxy rotation, respectively. In our models, nuclear spirals persist only in the region where $d(\Omega - \kappa/2)/dR < 0$, so that they should be trailing. They start out as tightly wound spirals and unwind with time as they become stronger to be nonlinear. This behavior of nonlinear growth and unwinding appears to be a generic properties of nonlinear spiral waves. Lee & Goodman (1999) found that the wavenumber of nonlinear waves is a decreasing function of the wave amplitude. Since nuclear spirals unwind faster when Q_b is larger, the probability of having more loosely wound spirals is smaller for galaxies with a stronger bar torque, which is consistent with the observational results of Peeples & Martini (2006).

5. Star formation in nuclear rings

We now focus on star formation in nuclear rings. We first summarize the observational results and then discuss the results of our numerical simulation.

5.1. *Observational perspectives*

Star formation is active in nuclear rings of barred galaxies. There are some observational results that can provide important information regarding how star formation proceed in nuclear rings. First, the observational data presented by Mazzuca *et al.* (2008) and Comerón *et al.* (2010) for a sample of nearby 17 galaxies indicate that the present-day star formation rate (SFR) of a nuclear ring appears related with the bar strength such

https://doi.org/10.1017/S174392131400012X Published online by Cambridge University Press

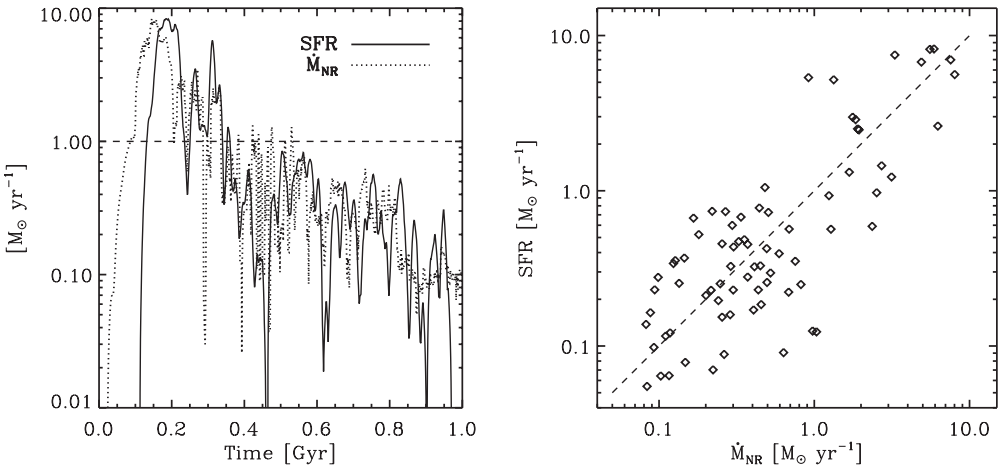

Figure 4. Left: Temporal evolution of (solid line) the SFR in the nuclear ring and (dotted line) the mass inflow rate $\dot{M}_{\rm NR}$ to the ring. **Right:** the relation between SFR and $\dot{M}_{\rm NR}$. The case with $\Sigma_0 = 20$ M$_\odot$ pc^{-2}, $f_{\rm bar} = 0.3$, and $\mathcal{R} = 2.5$ is shown. The dashed lines mark the SFR of 1 M$_\odot$ yr^{-1} in the left panel and SFR $= \dot{M}_{\rm NR}$ in the right panel. Adopted from Seo & Kim (2013).

that the SFR is quite small in strongly barred galaxies, while weakly barred galaxies have a wide range of the SFR between $\sim 0.1 - 10$ M$_\odot$ yr^{-1}, although the sample size is too small to make it conclusive.

Second, various population synthesis modelings of ring star formation show that the strength of observed emission lines from the nuclear rings is best described by multiple starburst activities occurring over a few Gyr (e.g., Allard *et al.* 2006 for NGC 4321; Sarzi *et al.* 2007 for NGC 4314 and NGC 7217), suggesting that ring star formation is long lived. Similarly, van der Laan *et al.* (2013) found that the circumnuclear ring in NGC 6951 has been forming stars for ~ 1 Gyr, despite at a low rate of ~ 0.1 M$_\odot$yr^{-1}. This may rule out the possibility that ring star formation is short lived with a single burst.

Third, the measurements of the equivalent widths of Hα lines indicate that some galaxies exhibit an age gradient of star clusters along the azimuthal direction of a nuclear ring, while many galaxies do not show a noticeable age gradient (Mazzuca *et al.* 2008; Ryder *et al.* 2010; Brandel *et al.* 2012). In galaxies with an age gradient, younger clusters are found preferentially near the contact points between the dust lanes and the nuclear ring, while older clusters are located systematically farther away from the contact points. To explain this, Böker *et al.* (2008) proposed two models of star formation in nuclear rings. The first one is called the "popcorn model" in which star formation takes place in dense clouds randomly distributed in a ring, so that no age gradient can be expected. This may happen when the ring is very massive to be gravitationally unstable. The second one is called the "pearls-on-a-string model" in which star formation occurs preferentially at the contact points. This may happen since the contact points formed by collisions of two steams of gas are densest in the ring. Since star clusters age as they orbit along the ring, this model naturally predicts a bipolar azimuthal age gradient of star clusters starting from the contact points. Statistically speaking, galaxies without age gradient have slightly larger SFR than galaxies with age gradients (Mazzuca *et al.* 2008). What controls the presence or absence of a azimuthal age gradient is an interesting question.

https://doi.org/10.1017/S174392131400012X Published online by Cambridge University Press

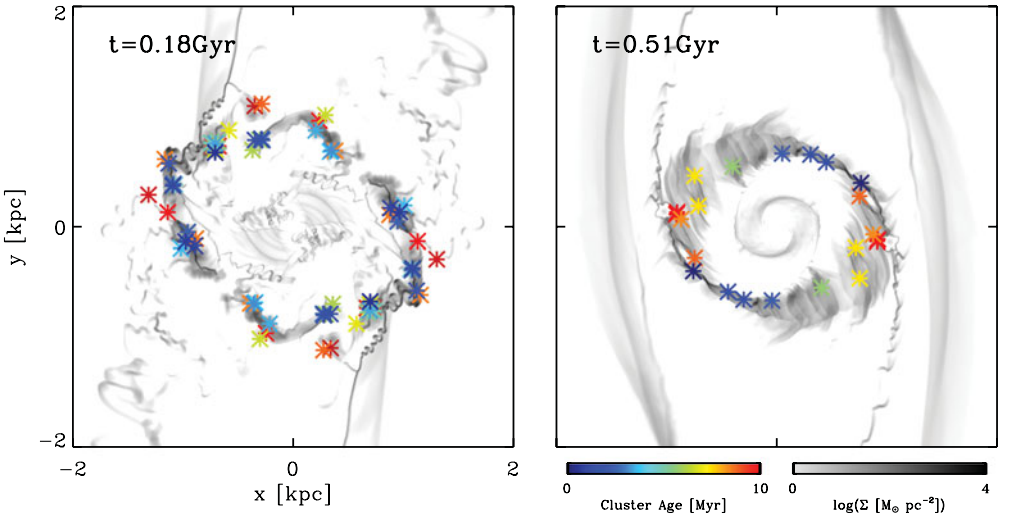

Figure 5. Distribution of (asterisks) young clusters with age less than 10 Myr at (**left**) $t = 0.18$ Gyr and (**right**) $t = 0.51$ Gyr, overlaid on the gas density distribution in greyscale, in the model with $\Sigma_0 = 20$ M$_\odot$ pc^{-2}, $f_{\rm bar} = 0.3$, and $\mathcal{R} = 2.5$. At $t = 0.18$ Gyr, clusters form randomly in the nuclear ring, while they form preferentially at the contact points at $t = 0.51$ Gyr. The color indicates the cluster ages, while the greyscale bar represents the gas surface density in logarithmic scale. Adopted from Seo & Kim (2013). [A color version is available online.]

5.2. *Numerical results*

In an attempt to understand the observational results summarized above, we have run numerical simulations with the effect of star formation and feedback included (Seo & Kim 2013). Figure 4(a) plots the evolution of (solid line) the SFR occurring in the nuclear ring and (dotted line) the mass inflow rate $\dot{M}_{\rm NR}$ to the ring, measured at $R = 2$ kpc, as functions of time. The results from the model with $\Sigma_0 = 20$ M$_\odot$ pc^{-2}, $f_{\rm bar} = 0.3$, and $\mathcal{R} = 2.5$ are shown. Figure 4(b) compares the SFR and $\dot{M}_{\rm NR}$ in the same model. Note that while there is some scatter, the SFR is linearly correlated with $\dot{M}_{\rm NR}$ over two orders of magnitude variation in them. This suggests that the ring SFR is determined primarily by the mass inflow rate rather than other factors such as the total gas mass in the ring. A slight offset of ~ 50 Myr between the histories of the SFR and $\dot{M}_{\rm NR}$ corresponds to the gas flow time from $R = 2$ kpc to the ring.

The SFR exhibits a primary burst with duration of 0.1 Gyr and subsequently a few secondary bursts before declining to very small values (less than 1 M$_\odot$ yr^{-1}). The primary burst is associated with the initial rapid gas infall due to the bar growth, while the secondary bursts are caused by the re-entry of the ejected gas from the star formation feedback of the primary burst. The primary reason for the very low SFR after the primary and secondary bursts is of course that only the gas inside the outermost x_1 orbit (with $x_c = 3.6$ kpc and $y_c = 4.7$ kpc) can lower its orbits strongly to initiate radial inflow, while the regions outside the outermost x_1 orbit are relatively unperturbed, as explained above. The total gas mass transforming to stars is 9×10^8 M$_\odot$ over 1 Gyr.

The presence or absence of an azimuthal age gradient of star clusters depends on the SFR (or the mass inflow rate to the ring) in our models, such that an age gradient exists when the SFR is lower than 1 M$_\odot$ yr^{-1}. This is because there is the maximum SFR that can be allowed at the contact points. For example, Figure 5 shows the spatial distribution of young clusters as asterisks with age less than 10 Myr, with the colorbar indicating their age, at $t = 0.18$ and 0.51 Gyr in the same model as in Figure 4. Note that

https://doi.org/10.1017/S174392131400012X Published online by Cambridge University Press

when $t = 0.18$ Gyr, the SFR is rather high at ~ 8.3 $M_\odot$ yr^{-1}, and young star clusters are distributed almost randomly along the ring, without showing an apparent azimuthal age gradient. In this case, $\dot{M}_{\rm NR}$ is so large that all the inflowing gas along the dust lanes cannot be consumed instantly at the contact points. The extra gas overflowing the contact points goes into the nuclear ring. The ring becomes massive and forms stars randomly in clumps that become dense enough, resulting in no age gradient. When $t = 0.51$ Gyr, on the other hand, the SFR is low at ~ 0.74 $M_\odot$ yr^{-1} and older clusters are located systematically farther away from the contact points. In this case, most of the inflowing gas can be converted to stars at the contact points, resulting in a well-defined azimuthal age gradient along the ring.

Allowing for the $\epsilon = 1\%$ of star formation efficiency during the free-fall time $\tau_{\rm ff}$, the maximum SFR afforded to the two contact points is given formally by

$$\dot{M}_{\rm crit} = 2\epsilon\Sigma_{\rm CP} R_{\rm ring} \Delta R \Delta\phi/\tau_{\rm ff}, \tag{5.1}$$

where $\Sigma_{\rm CP}$ is the gas surface density at the contact points, ΔR and $\Delta\phi$ are the radial and angular sizes of a contact point, respectively. In our models, $\Sigma_{\rm CP} = 4000$ $M_\odot$ pc^{-2}, $R_{\rm ring} = 1$ kpc, $\Delta R = 50$ pc, and $\Delta\phi = 30°$, leading to $\dot{M}_{\rm crit} \sim 1$ $M_\odot$ yr^{-1} in agreement with our numerical results. Notice however, that $\dot{M}_{\rm crit} \propto c_s^3 R_{\rm ring}^2$ assuming $\Delta R \propto R_{\rm ring}$. Thus, $\dot{M}_{\rm crit}$ may differ widely from galaxy to galaxy, suggesting that an absolute value of $\dot{M}_{\rm crit}$ does not determine the presence or absence of an azimuthal ages gradient. Galaxies with a weak bar and/or strong turbulence would have large $\dot{M}_{\rm crit}$.

In addition to the azimuthal age gradients, we also find that star clusters with ages in the range $\sim 10^7$–10^9 yr exhibit a positive radial age gradient, such that young clusters are located close to the nuclear ring, while old clusters are found away from the ring. In our models, the radial age gradient naturally arises since the nuclear ring becomes smaller in size with time as gas with lower angular momentum is added to the ring (Kim *et al.* 2012a). This makes star-forming regions gradually move radially inward.

6. Summary and discussion

We have presented the results of hydrodynamic simulations to study the formation of gaseous bar substructures focusing on nuclear rings as well as star formation in nuclear rings. We demonstrate that nuclear rings form not by resonances but by the centrifugal barrier that the inflowing gas cannot overcome. This naturally predicts that galaxies with stronger bars possess a smaller nuclear ring owing to a larger amount of angular momentum loss at dust-lane shocks. In our models with only a bar potential (without spiral arms), star formation in nuclear rings exhibits a short duration (~ 0.1 Gyr) of the primary burst followed by weak secondary bursts, after which the SFR stays quiescent for most of the time. This is because only the gas in the bar region can respond strongly to the bar potential to produce a rapid gas infall at early time. As the gas in the bar region becomes evacuated, the mass inflow rate and SFR become very small. An azimuthal age gradient of star clusters is expected when the SFR is less than the critical value $M_{\rm crit}$ defined by equation (5.1) (corresponding to ~ 1 $M_\odot$ yr^{-1} for our model parameters) affordable at the contact points, since star-forming regions are located preferentially at the contact points.

Very recently, Piñol-Ferrer *et al.* (2014) presented a dynamical model of NGC 1097 that successfully matches the observed density distribution and kinematic map in detail. They concluded that the nuclear ring with radius $R_{\rm ring} \sim 1$ kpc is nowhere close to the

https://doi.org/10.1017/S174392131400012X Published online by Cambridge University Press

ILR radii located at 60 pc and 2.9 kpc, which is seemingly consistent with our numerical results showing that the ring formation has nothing to do with the ILR.

Our numerical results show that the SFR stays very small for most of the evolutionary time except for the some bursts lasting only for ~ 0.1 Gyr. This is in contrast to the observational results mentioned above (e.g., Allard *et al.* 2006; Sarzi *et al.* 2007). If the ring star formation is truly a long lived phenomenon, our numerical results suggest that the fresh gas should be supplied continuously or continually to the bar region for sustained star formation. Candidate mechanisms for gas feeding to the bar region include the angular momentum loss by spiral arms, and gas accretion in the form of galactic fountains (Fraternali & Binney 2006, 2008) or cosmic infall of the primordial gas (e.g., Dekel *et al.* 2009). Observations show that high velocity clouds feed a normal disk galaxy with gas at a rate ~ 0.7 $M_\odot$ yr^{-1} (Richter 2012). It will be interesting to study how these processes affect star formation in nuclear rings.

Acknowledgements

This work was supported by the National Research Foundation of Korea (NRF) grant funded by the Korean government (MEST), No. 2010-0000712. The computation of this work was supported by the Supercomputing Center/Korea Institute of Science and Technology Information with supercomputing resources including technical support (KSC-2012-C3-19).

References

Athanassoula, E. 1992, *MNRAS* 259, 345
Böker, T., Falcón-Barroso, J., Schinnerer, E., *et al.* 2008, *AJ* 135, 479
Buta, R. & Combes, F. 1996, *Fund. Cosmic Phys.* 17, 95
Combes F. & Gerin M. 1985, *A&A* 150, 327
Combes, F. & Sanders, R. H. 1981, *A&A* 96, 164
Comerón, S., Martínez-Valpuesta, I., Knapen, J. H., & Beckman, J. E. 2009, *ApJ* 706, L256
Comerón, S., Knapen, J. H., Beckman, J. E., *et al.* 2010, *MNRAS* 402, 2462
Dekel, A., Sari, R., & Ceverino, D. 2009, *ApJ* 703, 785
Fraternali, F. & Binney, J. 2006, *MNRAS* 366, 449
Fraternali, F. & Binney, J. 2008, *MNRAS* 386, 935
Hsieh, P.-Y., Matsushita, S., Liu, G., Ho, P. T. P., Oi, N., & Wu, Y.-L. 2011, *ApJ* 736, 129
Kim, C.-G., Kim, W.-T., & Ostriker, E. C. 2011, *ApJ* 743, 25
Kim, W.-T. & Stone, J. M. 2012, *ApJ* 751, 124
Kim, W.-T., Seo, W.-Y., & Kim, Y. 2012a, *ApJ* 758, 14
Kim, W.-T., Seo, W.-Y., Stone, J. M., Yoon, D., & Teuben, P. J. 2012b, *ApJ* 747, 60
Knapen, J. H., Pérez-Ramìrez, D., & Laine, S. 2002, *MNRAS* 337, 808
Laurikainen, E. & Salo, H. 2002, *MNRAS* 337, 1118
Lee, E. & Goodman, J. 1999, *MNRAS* 308, 984
Lee, G.-H., Park, C., Lee, M. G., & Choi, Y.-Y. 2012, *ApJ* 747, 125
Martini, P., Regan, M. R., Mulchaey, J. S., & Pogge, R. W. 2003, *ApJ* 589, 774
Masters, K. L., Nichol, R. C., Hoyle, B., *et al.* 2011, *MNRAS* 411, 2026
Mazzuca, L. M., Knapen, J. H., Veilleux, S., & Regan, M. W. 2008, *ApJ* 174, 337
Mazzuca, L. M., Swaters, R. A., Knapen, J. H., & Veilleux, S. 2011, *ApJ* 739, 104
Peeples, M. S. & Martini, P. 2006, *ApJ* 652, 1097
Pfenniger, D. 1984, *A&A* 134, 373
Piner, B. G., Stone, J. M., & Teuben, P. J. 1995, *ApJ* 449, 508
Piñol-Ferrer, N., Fathi, K., Carignan, C., *et al.* 2014, *MNRAS* 438, 971
Prieto, M. A., Maciejewski, W., & Reunanen, J. 2005, *AJ* 130, 1472
Richter, P. 2012, *ApJ* 750, 165

Sanders, R. H. & Huntley, J. M. 1976, *ApJ* 209, 53
Seo, W.-Y. & Kim, W.-T. 2013, *ApJ* 769, 100
Sheth, K., Elmegreen, D. M., Elmegreen, B. G., *et al.* 2008, *ApJ* 675, 1141
Shlosman, I., Begelman, M. C., & Frank, J. 1990, *Nature* 345, 679
Shull, J. M. 1980, *ApJ* 237, 769
van der Laan, T. P. R., Schinnerer, E., Emsellem, E., *et al.* 2013, *A&A* 551, A81
van de Ven, G. & Fathi, K. 2010, *ApJ* 723, 767

https://doi.org/10.1017/S174392131400012X Published online by Cambridge University Press